BJP British Journal of Pharmacology

DOI:10.1111/bph.12947
www.brjpharmacol.org

RESEARCH PAPER

Sonic hedgehog increases the skin wound-healing ability of mouse embryonic stem cells through the microRNA 200 family

Han Na Suh and Ho Jae Han

Department of Veterinary Physiology, College of Veterinary Medicine and Research Institute for Veterinary Science, Seoul National University, Seoul, South Korea

Correspondence
Ho Jae Han, Department of Veterinary Physiology, College of Veterinary Medicine, Seoul National University, Gwanak-ro, Gwanak-gu, Seoul, 151-742, South Korea. E-mail: hjhan@snu.ac.kr

Received
29 May 2014
Revised
3 September 2014
Accepted
13 September 2014

BACKGROUND AND PURPOSE

To use stem cell therapy effectively, it is important to enhance the therapeutic potential of stem cells with soluble factors. Although sonic hedgehog (shh) is important in maintaining the stem cell, the recovery effect of mouse embryonic stem cells (mESCs) with shh has not yet been elucidated. The present study investigated the effect of mESCs with shh in skin recovery *in vivo* as well as the related intracellular signal pathways *in vitro*.

EXPERIMENTAL APPROACH

The healing effect of mESCs with shh on skin wounds was examined *in vivo* in ICR mice. The involvement of Smads, the microRNA (miR)-200 family, zinc finger E-box-binding homeobox (ZEBs) and E-cadherin on shh-induced mESC migration and self-renewal was determined *in vitro*.

KEY RESULTS

The mESCs with shh increased re-epithelialization and VEGF expression in skin wounds. Shh-treated mESCs increased both secreted and intracellular levels of VEGF. Shh induced dephosphorylation of glycogen synthase kinase 3β through the Smoothened receptor and increased the phosphorylation of Smad1 and Smad2/3 in mESCs. Shh-induced decrease of the mmu-miR-141, -200c, -200a, -200b and -429 expression levels was significantly reversed by Smad4 siRNA. Shh increased nuclear expression of ZEB1/ZEB2 and decreased E-cadherin expression while increasing cell migration and skin wound healing. Both these effects were reversed by mmu-miR-141 and -200b mimics.

CONCLUSIONS AND IMPLICATIONS

Mouse ESCs accelerated skin wound healing by shh through down-regulating E-cadherin, an effect dependent on mmu-miR-141 and -200b. Our data provides evidence for the effectiveness of shh in stem cell-based therapy *in vivo*.

Abbreviations

GSK3β, glycogen synthase kinase 3β; LIF, leukaemia inhibitory factor; mESC, mouse embryonic stem cell; shh, sonic hedgehog; SMO, Smoothened receptor; ZEB, zinc finger E-box-binding homeobox

Tables of Links

TARGETS
Enzymes[a]
GSK3β, glycogen synthase kinase 3
GPCR[b]
SMO, Smoothened receptor

LIGANDS
VEGF

These Tables list key protein targets and ligands in this article which are hyperlinked to corresponding entries in http://www.guidetopharmacology.org, the common portal for data from the IUPHAR/BPS Guide to PHARMACOLOGY (Pawson *et al.*, 2014) and are permanently archived in the Concise Guide to PHARMACOLOGY 2013/14 ([a,b]Alexander *et al.*, 2013a,b).

Introduction

Skin wound healing is a well-organized process of cell migration and proliferation that involves extracellular matrix deposition, angiogenesis, and tissue remodelling. Besides self-renewal, stem cells promote wound healing and reduce inflammation (Wu *et al.*, 2007). Although the mechanism underlying stem cell-induced skin wound healing is not fully understood, stem cells play key roles in wound neovascularization, wound contraction, keratinization and recovery (Liu *et al.*, 2008). Additionally, stem cells secrete various growth factors, cytokines, chemokines and bioactive lipids into the micro-environment in an autocrine/paracrine manner (Guo and Dipietro, 2010; Ratajczak *et al.*, 2012). Despite limitations in embryonic stem cells (ESCs) for skin wound healing, a previous study reported that mouse ESCs (mESCs) reconstitute into fully differentiated skin (Coraux *et al.*, 2003) and the topical application of ESCs enhance skin wound healing in diabetic rats (Lee *et al.*, 2011) as well as the mesenchymal stem cells (MSCs) recovered through the paracrine manner of biological active molecules (Chen *et al.*, 2008). Therefore, the complex interaction of stem cells and soluble factors in wound sites has been examined through an *in vitro* study.

Recent studies refer to the hedgehog proteins in regulation of primitive haematopoietic cells (Bhardwaj *et al.*, 2001), mammary stem cells (Liu *et al.*, 2006) and neural stem cell (Ahn and Joyner, 2005) involved in adult tissue maintenance and regeneration. Although the three hedgehog proteins in vertebrates – sonic hedgehog (shh), Indian hedgehog and desert hedgehog (dhh) – are highly homologous and share receptors and intracellular signal pathways (Carpenter *et al.*, 1998; Johnson and Scott, 1998), their potency and function differ. Shh knockout leads to embryonic death in mice (Chiang *et al.*, 1996) while dhh knockout animals had minor defects (Bitgood *et al.*, 1996). Shh is the most widely expressed and potent and it affects the cells in an autocrine/paracrine manner (Delloye-Bourgeois *et al.*, 2013). Shh stimulates mESC proliferation in an undifferentiation status (Heo *et al.*, 2007) and directly controls the migration of various cell types (Hochman *et al.*, 2006; Yoo *et al.*, 2008). The hypervascularization of the neuroectoderm depends on shh overexpression in the dorsal neural tube (Rowitch *et al.*, 1999), but the mechanisms underlying the interactions between ESCs migration or proliferation and angiogenesis in the presence of shh in skin wounds need to be elucidated .

The cell–cell interaction is a direct reciprocal action between the cell–cell surfaces that maintains stability through various cell junctions (Tepass and Harris, 2007) and several experiments suggest that adhesion molecules regulate stemness, although none are conclusive as it is difficult to exclude non-cell autonomous effects (Marthiens *et al.*, 2010). While E-cadherin is an undifferentiated marker that identifies hESCs (D'Amour *et al.*, 2005; Eastham *et al.*, 2007), FBS and leukaemia inhibitory factor (LIF) in media maintain the undifferentiated status of E-cadherin –/– ES cells (Spencer *et al.*, 2007; Ying *et al.*, 2008). Various microRNAs (miRNAs) target the cell architecture components of tight junctions and of adherent junctions (Lamouille *et al.*, 2013) and the miR-200 family inhibits ESC differentiation by directly targeting Cadherin11 and Neurophilin1 (Lin *et al.*, 2009). The miRNA target prediction algorithms showed that the zinc finger E-box-binding homebox 1 (ZEB1) and ZEB2, the most conspicuous targets of the miR-200 family, are transcriptional repressors of E-cadherin and are regulators of cell adhesion (Burk *et al.*, 2008; Korpal *et al.*, 2008). Therefore, the miR-200 family-mediated cadherin regulation might be important in maintaining ESC. Although similar miRNA expression in undifferentiated mouse and human stem cells suggests that the miRNAs play an important role in ESC pluripotency and differentiation (Suh *et al.*, 2004; Calabrese *et al.*, 2007; Lin *et al.*, 2009), the exact role of the miR-200 family in self-renewal has yet to be determined. The present study examined the effects of mESC and any synergy with shh on the healing of skin wounds *in vivo*, as well as the *in vitro* intracellular signal mechanisms.

Methods

Mouse skin wound healing model

All animal care and experimental procedures followed the standard operating protocols of Seoul National University and were approved by the Institutional Review Board at Seoul National University. In addition, authors are Doctors of Veterinary Medicine with licenses granted from the Ministry of Agriculture, Food and Rural Affairs of the Republic of Korea. All studies involving animals are reported in accordance with the ARRIVE guidelines for reporting experiments involving animals (Kilkenny *et al.*, 2010; McGrath *et al.*, 2010). A total of 78 animals were used in the experiments described here.

Seven-week-old male ICR mice were purchased from Han Lim Experimental Animal (Suwon, Korea). Methods for mouse skin excision wound splinting model and stem cell transplantation were as described in an earlier study (Wang *et al.*, 2013). Mice were randomly divided into groups ($n = 6$, each group). Mice were anaesthetized(i.p. injection) using a combination of Zoletil 50®, Rompun® and saline (a ratio of 2:1:2, respectively) and placed on a heating table kept at 37°C to maintain constant body temperature. The back was shaved, sterilized with povidone iodine followed by 70% ethanol and a wound was created by using a 6 mm diameter sterile biopsy punch surgically. In the cell-treated group, cells (0.7×10^6 mESCs in 60 µL saline) were injected into the dermis at four sites around the wound. We also topically applied 0.3×10^6 mESCs in 20 µL Matrigel (BD Biosciences, San Jose, CA, USA) onto the wound site. In the mESCs with shh group, cells were pre-activated with shh for 24 h and then mESCs were applied with shh. A splint was placed around the wound (with several stitches and/or glue) and dressed with Tegaderm (3M) sterile transparent dressing. Mice were placed in individual cages in a warm and humid incubator. Images of wound were acquired on day 0, 1, 5, 7, 8, 9 with a digital camera system (40D, Canon, Tokyo, Japan) at the same distance. At day 9, the wound tissues were embedded in OCT compound (Sakura Finetek, Torrance, CA, USA), stored at −70°C, cut 6 µm frozen sections using cryosectioning machine and mounted on SuperFrost Plus slides (Thermo Fisher Scientific, Waltham, MA, USA) for haematoxylin and eosin staining. Applying mESCs as stem cell therapy can have the negative effects like teratoma formation and immune rejection. However, previous studies suggest that teratoma formation is dependent upon experimental conditions (Asano *et al.*, 2003; Mitjavila-Garcia *et al.*, 2005). Moreover, Lee *et al.* (2011) applied mESCs onto wounded skin for 20 days without teratoma formation and immune rejection. To support the scientific evidence of a lack of immune rejection in our study, we examined the expression level of IFN-γ and TNF-α in skin tissue. Among the groups (vehicle, shh, mESCs, mESCs with shh), the expression level of both IFN-γ and TNF-α made no difference (Supporting Information Fig. S1). This result suggests that the negative effects of stem cell application onto skin wound could be ruled out in our experimental conditions.

MESC culture

Mouse ESCs were cultured on the gelatin coated culture dish in DMEM (Gibco-BRL, Gaithersburg, MD, USA) supplemented with 3.7 g·L^{-1} sodium bicarbonate, 1% penicillin/streptomycin, 1.7 mM L-glutamine, 0.1 mM β-mercaptoethanol, 5 ng·mL^{-1} mouse LIF and 15% FBS at 37°C incubator with 5% CO_2. The medium was changed to serum-free standard medium (5% serum replacement instead of 15% FBS) for 24 h prior to experiment.

Subcellular fractionation

Cells were dissolved in buffer A [137 mM NaCl, 8.1 mM Na_2HPO_4, 2.7 mM KCl, 1.5 mM KH_2PO_4, 2.5 mM EDTA, 1 mM dithiothreitol, 0.1 mM phenylmethanesulfonylfluoride, 10 µg·mL^{-1} leupeptin (pH 7.5)] and lysates were first centrifuged at 1000× *g* for 10 min at 4°C. Cytosolic and total particulate fractions were then prepared by centrifuging the supernatants at 100 000× *g* for 1 h at 4°C. The supernatants (cytosolic fraction) were then precipitated with acetone, incubated for 5 min on ice and centrifuged at 20 000× *g* for 20 min at 4°C. Pellets were resuspended in buffer A containing 1% (v/v) Triton X-100. The particulate fractions containing the membrane fraction were resuspended in buffer A containing 1% (v/v) Triton X-100. Protein was quantified using the Bradford procedure.

Immunoblot and immunoprecipitation

For immunoblot, cell lysates (20–40 µg) were separated using various percentages (6–15%) of SDS-polyacrylamide gel electrophoresis (SDS-PAGE) and transferred to PVDF membranes. Each membrane was incubated with 5% skim milk, appropriate primary antibody and HRP-conjugated secondary antibody. For immunoprecipitation, cell lysates were incubated with target antibody-binding protein A/G-sepharose beads and then gently shaken for 12 h at 4°C. SDS-PAGE sample buffer was added into beads and boiled at 100°C for 5 min to release the protein and then immunoblot was performed with target antibody. Bands were visualized with an enhanced chemiluminescence and then images were acquired for quantitative analysis with ChemiDoc™ XRS$^+$ System (Biorad, Hercules, CA, USA).

Cellular delivery of small interfering ribonucleic acid (siRNA) and miRNA

Cells were transfected for 24 h with a SMARTpool of siRNAs specific to VEGF (cat# L-040812), Smad1 (cat# L-055762), Smad3 (cat# L-040706), Smad4 (cat# L-040687), ZEB1 (cat# L-051513-01) or non-targeting (Nt) siRNAs (cat# D-001206; as a negative control; Dharmacon, Lafayette, CO, USA) using Dharmafect transfection reagent (Dharmacon). Cells were transfected for 24 h with mmu-miR-141 mimic (cat# C-310418-05), mmu-miR-141 hairpin inhibitor (cat# IH-310418-07), mmu-miR-200b mimic (cat# C-310456-07), mmu-miR-200b hairpin inhibitor (cat# IH-310418-07), miR hairpin inhibitor negative control (cat# IN-001005-01) or miR mimic negative control (cat# CN-001000-01; Dharmacon) using Dharmafect transfection reagent. Transfection efficiency of siRNAs was examined using immunoblot (Supporting Information Fig. S2). The effect of mimic negative control and hairpin inhibitor negative control itself was examined using Oris™ migration assay (Supporting Information Fig. S3).

Immunofluorescence staining

Cells were fixed with 3.5% paraformaldehyde, the permeability increased with 0.1% Triton X-100, blocked with 5% BSA, and then treated with primary antibody against the target protein (1:50). Cells was then incubated with FITC-conjugated secondary antibody (1:100) for 30 min and PI (10 µg·mL^{-1}) was added for 15 min. Fluorescence images were visualized with a FluoView ×300 fluorescence microscope (Olympus, Tokyo, Japan).

Measurement of miRNA expression using reverse transcriptase-quantitative PCR (qRT-PCR)

Total RNA was extracted from mESCs using a RNeasy Plus Mini Kit (Qiagen, Hilden, Germany). Cells were harvested, disrupted by adding Buffer RLT Plus and homogenized by passing through a 20-gauge needle. Homogenized lysate was transferred to a gDNA Eliminator spin column and centrifuged for 30 s at 8000× *g*. Flow-through solution was added (1 volume of 70% ethanol and transferred to an RNeasy spin column and then centrifuged for 15 s at 8000× *g* RNeasy spin column was washed by buffer RW1 and then buffer RPE. RNA was extracted by RNase-free water. The miRNA expression level was measured according to manufacturer's protocol. cDNA synthesis was performed using NCode™ VILO™ miRNA cDNA synthesis kit (Invitrogen, cat#A11193-05) and then expression of miRNAs was detected in a Rotor-Gene 6000 real-time thermal cycling system using the NCode express SYBR GreenER™ miRNA qRT-PCR kit universal (cat# A11193-51). Used miRNA-specific primers were as following; miR-141: 5′-TAACACTGTCTGGTAAAGATGG-3′, miR-200c: 5′-TAATACTGCCGGGTAATGATGG-3′, miR-200a: 5′-TAACACTGTCTGGTAACGATGT-3′, miR-200b: 5′-TAATAC TGCCTGGTAATGATGA-3′, miR-429: 5′-TAATACTGTCTGG TAATGCCGT-3′. Universal qPCR primer was supplied in NCode express SYBR GreenER miRNA qRT-PCR kit universal.

Chromatin immunoprecipitation (ChIP)

Cells were fixed with 1% formaldehyde for 10 min at room temperature and then quenched with 125 mM glycine. Cells were washed in PBS and resuspended in 300 μL SDS lysis buffer [50 mM Tris-HCl (pH 8.8), 10 mM EDTA, 1% SDS and protease inhibitors] and kept on ice for 20 min. The chromatin was sonicated 12 times in 10 s pulses to yield DNA fragments with an average length of ~ 500 bp. After centrifugation at 18 000× *g* for 10 min, the supernatants were diluted with dilution buffer [50 mM Tris-HCl (pH 8.8), 1.1% Nonidet P-40, 167 mM NaCl and protease inhibitors]. 10 μL chromatin lysates were acquired as Input. Lysates were pre-cleared with protein G agarose and subsequently incubated with positive control (anti-RNA polymerase II), negative control (normal rabbit IgG) and ZEB1 (rabbit polyclonal antibody) at 4°C overnight. Fresh beads were then added to immunoprecipitated chromatin for 2 h and washed in low salt, high salt, LiCl and TE buffer subsequently. DNA/protein complex crosslinking was reversed by heating overnight at 65°C and treated with proteinase K and RNase A. DNA fragments were then purified in Bind Reagent 'A' using Collecting Tube. All materials were acquired from Millipore (EZ-ChIP™ cat# 17–371) and experiments were performed, following the manufacturers' protocol.

ChIP and qPCR analysis

Each PCR reaction was performed in triplicate in 20 μL reaction volumes containing ChIP-enriched or input DNA, Power SYBR Green master mix, region specific primer sets (Mm cdh1 PRMT LP: 5′-CATGCTGGGCTACATAGCAA-3′, Mm cdh1 PRMT RP: 5′-TGGGCCTGGAATTGTCTTAG-3′) and distilled water. Target amplification and detection was performed by Rotor-Gene 6000 cycler. Specificity of the PCR reactions was confirmed by electrophoresis and dissociation curve analysis. The expression level was normalized to GAPDH and calculated relative to control.

Cell migration assay

Oris assay. Cells were seeded at 3×10^2 cells·100 μL^{-1} in each well (Platypus Technologies, Madison, WI, USA; cat# CMA 1. 101). Inserts were carefully removed when cells had reached 70% confluence and treated with shh, miRNAs or siRNAs. Then, migrated cells were stained with 5 μM calcein-AM and quantified through measurement of fluorescence signals using a microplate reader at excitation and emission wavelengths of 485 and 515 nm respectively.

Wound-healing assay. Cells were seeded at 4×10^4 cells·200 μL^{-1} in culture dishes with inserts (Ibidi, Munich, Germany). After 70% confluence, inserts were removed to create a wound field of approximately 500 μm and cells were incubated with shh or miRNAs. Cells were stained using Diff-Quik staining and migration distance was measured.

Live cell imaging microscopy. Cells were placed in chambers with controlled temperature and CO_2 (Tokai, Tokyo, Japan) with or without shh, installed in a Olympus IX81-ZDC zero-drift microscope. A series of images were acquired for 0–24 h at 5 min intervals, using a Cascade 512B camera (Roper Scientific, Tucson, AZ, USA) operated by the multidimensional acquisition package of MetaMorph v. 7.01 software (Molecular Devices, Sunnyvale, CA, USA).

Propidium iodide PI staining and cell cycle analysis

Cells were dissociated in 0.05% trypsin/EDTA, resuspended in PBS containing 0.1% BSA (10^6 cells·1 mL^{-1}) and fixed with 70% ice-cold ethanol for 30 min at 4°C. Fixed cells were incubated with 250 μg·mL^{-1} PI and 100 μg·mL^{-1} RNase for 30 min at 37°C to stain the DNA. Cell cycle histograms were generated after analysing the PI-stained cells by FACS (Beckman Coulter, Fullerton, CA, USA). Samples were analysed using CXP software (Beckman Coulter) and proliferation index $[(S + G2/M)/(G0/G1 + S + G2/M)] \times 100$ were calculated.

Data analysis

All results are expressed as mean ± SD. All experiments were analysed by one-way ANOVA. Several experiments were also evaluated by comparing the treatment means to the control using a Bonferroni–Dunn test. Statistical significance was defined at $P < 0.05$.

Materials

Mouse ESCs (ES-E14TG2a) were obtained from the American Type Culture Collection (Manassas, VA, USA). FBS was purchased from Gibco (Rockville, MD, USA). Ssh, cyclopamine, lithium chloride (LiCl), primary antibody against ZEB2 (cat#, SAB3500515; dilution, 1:1000) and fluorescein isothiocyanate (FITC)-anti-rabbit antibody (cat#, F9887; dilution, 1:100) were purchased from Sigma-Aldrich (St. Louis, MO, USA). Propidium iodide (PI) was obtained from Invitrogen (Carlsbad, CA, USA). LIF, purmorphamine, primary

antibodies against VEGF (cat#, sc-7269; dilution, 1:1000), cyclinE (cat#, sc-481; dilution, 1:1000), CDK2 (cat#, sc-748; dilution, 1:1000), cyclin D1 (cat#, sc-753; dilution, 1:1000), CDK4 (cat#, sc-749; dilution, 1:1000), glycogen synthase kinase 3β (GSK3β; cat#, sc-9166; dilution, 1:1000), p-GSK3β (cat#, sc-11757; dilution, 1:1000), p-Smad1 (cat#, sc-12353; dilution, 1:1000), p-Smad2/3 (cat#, sc-11769; dilution, 1:1000), Smad4 (cat#, sc-7966; dilution, 1:1000), Smad (cat#, sc-7153; dilution, 1:1000), ZEB1 (cat#, sc-25388; dilution, 1:1000), E-cadherin (cat#, sc-7870; dilution, 1:1000), Snail1 (cat#, sc-28199; dilution, 1:1000), β-catenin (cat#, sc-7963; dilution, 1:1000), ZO-1 (cat#, sc-10804; dilution, 1:1000), occludin (cat#, sc-5562; dilution, 1:1000), Cx43 (cat#, sc-9059; dilution, 1:1000), Lamin A/C (cat#, sc-20681; dilution, 1:1000), β-actin (cat#, sc-47778; dilution, 1:1000) and secondary antibodies against HRP-conjugated goat anti-rabbit IgG (cat#, sc-2004; dilution, 1:10 000), goat anti-mouse IgG (cat#, sc-2005; dilution, 1:10 000), rabbit anti-goat IgG (cat#, sc-2768; dilution, 1:10 000) were obtained from Santa Cruz Biotechnology (Santa Cruz, CA, USA). All other reagents were of the highest purity commercially available.

Results

Role of mESCs with shh on skin wound healing

To examine the effects of mESCs on skin wound healing, four groups of mice were prepared – vehicle, shh, mESCs and mESCs with shh (mESCs + shh). Soluble factors such as shh are thought to accelerate tissue regeneration by stem cells, so the skin wound was treated by shh, mESCs or mESCs with shh separately. We measured the wound size on days 0, 1, 5, 7, 8 and 9 until epithelialization was complete in the group treated with mESCs and shh. Macroscopically, after day 5, shh, mESCs and mESCs with shh showed significant wound closure compared with the vehicle. In addition, the recovery rate was faster in mESCs with shh (Figure 1A). Figure 1B shows a representative skin wound at day 9 after wounding. Histologically, the mESCs with shh group showed an increase in re-epithelialization while the shh group and mESCs group showed incomplete restoration in the granular layer. The mESCs with shh healed *in vivo* (Figure 1A and B), but to identify the mESC factor that enhances skin wound healing, we assayed the angiogenic factor, VEGF, in mESCs and skin wound. Shh increased VEGF expression in mESCs along with secretion into medium (Figure 1C). Moreover, there was greater VEGF expression in the wounds treated with mESCs with shh that in those treated with mESCs only (Figure 1D). To examine the effect of VEGF on skin wounds, we applied VEGF siRNA-transfected mESCs in the presence or absence of shh. Compared with the mESCs group, the VEGF siRNA-transfected mESCs group (VEGF siRNA + mESCs) showed incomplete re-epithelization. However, VEGF siRNA-transfected mESCs with shh group (VEGF siRNA + mESCs + shh) showed complete re-epithelization with incomplete granular layer restoration. The Nt siRNA-transfected mESC with shh group (Nt siRNA + mESCs + shh) showed complete skin wound healing (Figure 1E). Our data demonstrated that mESCs with shh significantly enhanced VEGF expression, which provided a mechanistic explanation for VEGF's role in skin wound healing.

Role of shh in mESC migration and proliferation

Next, we examined the related intracellular mechanisms *in vitro*. To determine the role of shh on stem cell self-renewal, we examined cell migration and proliferation under the influence of shh (500 $ng \cdot mL^{-1}$). The Oris cell migration assay showed that shh increased the calcein-AM fluorescence, which indicates cell migration into denuded areas (Figure 2A). The *in vitro* wound-healing assay also showed that shh increased the migration distance (Figure 2B). Moreover, the live cell migration microscopy result showed that shh increased mESC motility and colony size, suggesting that shh affected the proliferation and migration (Figure 2C). Cell cycle analysis using PI staining showed that shh increases the proliferation index [control (non-treated): 49.5 ± 8.1%; shh: 68.3 ± 11.5%] (Figure 2D) and immunoblot of the cell cycle regulatory proteins (cyclin E, CDK2, cyclin D1, CDK4), which confirmed increased proliferation after shh (Figure 2E). To elucidate the signal pathways involved in shh-mediated migration and proliferation, we examined the receptor-related signal pathways. Shh stimulated dephosphorylation and activation of GSK3β time-dependently (≥12 h; Figure 2F) and these effects were blocked by the Smoothened receptor (SMO) inhibitor (cyclopamine). The SMO agonist (purmorphamine) showed a similar response to the shh (Figure 2G), suggesting that GSK3β activation is mediated by SMO. In order to determine the downstream signal pathways of GSK3β, Smads (Smad1 and Smad2/3) were measured. Shh increased the phosphorylation of both Smad1 and Smad2/3, which were inhibited by the GSK3β inhibitor (LiCl; Figure 2H and I). Cells were transfected with Smad siRNAs to determine the relationship between the intracellular signal pathway and VEGF synthesis. An endogenous depletion of Smad1, Smad3 or Smad4 decreased the VEGF secretion into medium and intracellular VEGF expression levels, which strongly suggested that VEGF synthesis was mediated by Smads (Figure 2J).

Effect of shh on miR-200 family expression

As Smads are well known miRNA regulators, we examined the involvement of Smads in the expression of the miR-200 family (mmu-miR-141, -200c, -200a, -200b and -429). Mmu-miR-141, -200c, -200a, -200b and -429 were expressed at similar levels in control cells while shh significantly decreased the miRNAs expression (Figure 3A). Smads are composed of R-Smad (Smad1/5 and Smad 2/3) and Co-Smad (Smad4; Blahna and Hata, 2012), so to determine the Smad involved in miR expression, we transfected the cells with Smad1, Smad3, Smad4 siRNAs (specific target) or Nt siRNA (negative control). The shh-induced decrease in miRNA expression was significantly reversed by Smad4 siRNA. Smad1 or Smad3 depletion slightly increased miRNA expression (Figure 3B). Therefore, shh exerts a negative regulation on the transcription of the miR-200 family, through R-Smad (Smad1, Smad2/3)/Co-Smad (Smad4) heterodimer formation.

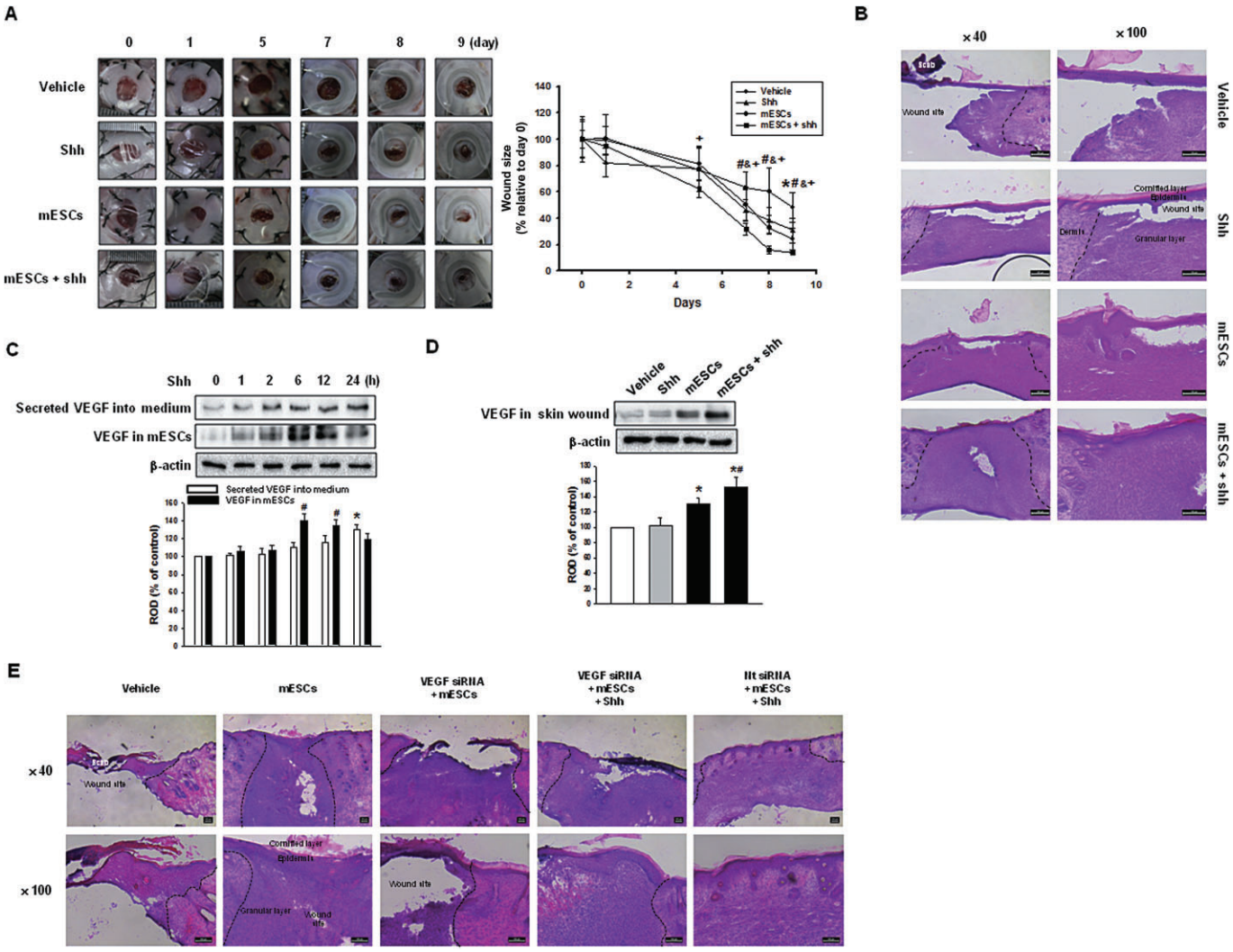

Figure 1

Role of mESCs with shh on skin wound healing *in vivo*. Vehicle, shh, mESCs or mESCs with shh (mESCs + shh) were applied to the skin wound. (A) Representative appearance of wound tretated with vehicle, shh, mESCs, or mESCs + shh at days 0, 1, 5, 7, 8, 9 (left panel). Quantification of wound size relative to original wound size (day 0) is calculated (right panel). Data represents the mean ± SD (n = 6). *P < 0.05 versus day 0 of vehicle; $^{\#}P$ < 0.05 versus day 0 of shh; $^{\&}P$ < 0.05 versus day 0 of mESCs; ^{+}P < 0.05 versus day 0 of mESCs + shh. (B) Representative haematoxylin and eosin (H&E) staining of wound skin at day 9 after wounding (n = 6). Scale bar = 200 μm. (C) mESCs were treated with shh for various time (0–24 h), and the secreted VEGF into medium and the expression of VEGF in mESCs were detected by immunoblot. The lower panel depicts the mean ± SD of three independent experiments for each condition, as determined from densitometry relative to β-actin. *P < 0.05 versus 0 h of secreted VEGF into medium; $^{\#}P$ < 0.05 versus 0 h of VEGF in mESCs. (D) The expression of VEGF was in wound skin at day 9 after wounding was determined by immunoblot. The lower panel depicts the mean ± SD of three independent experiments for each condition, as determined from densitometry relative to β-actin. *P < 0.05 versus vehicle; $^{\#}P$ < 0.05 versus mESCs. (E) Vehicle, mESCs, VEGF siRNA-transfected mESCs [VEGF siRNA (20 nM) + mESCs], VEGF siRNA-transfected mESCs with shh (VEGF siRNA + mESCs + shh) or Nt siRNA-transfected mESCs with shh (Nt siRNA + mESCs + shh) were applied to the skin wound. Representative H&E staining of wound skin at day 9 after wounding. Scale bar = 100 μm.

ZEB1/E-cadherin-mediated mESC migration via miR-200 family

The miRNA 200 family is classified into two subgroups: functional and genetic. Functionally, miR-200a, -141 (AACACUG), and miR-200b, -200c, -429 (AAUACUG) have different seed sequences. Genetically, miR-200a, -200b, -429 and miR-141, -200c are located in two gene clusters on two different chromosomes (Park *et al.*, 2008). Each group, miR-200b/200c/429 and miR-141/200a, has the same function targeting ZEB1/2. We chose miR-141 and miR-200b in this study since they can represent both subgroups in functional and genetic aspects. We then examined the relationship between mmu-miR-141, -200b and ZEBs. Shh and mmu-miR-141, -200b hairpin inhibitor increased both ZEB1 and ZEB2 protein expression in nucleus, whereas the mmu-miR-141, -200b mimic abolished the shh-mediated increase in ZEBs proteins. This modulation of miRNA expression might affect expression of ZEB proteins. However, E-cadherin levels were

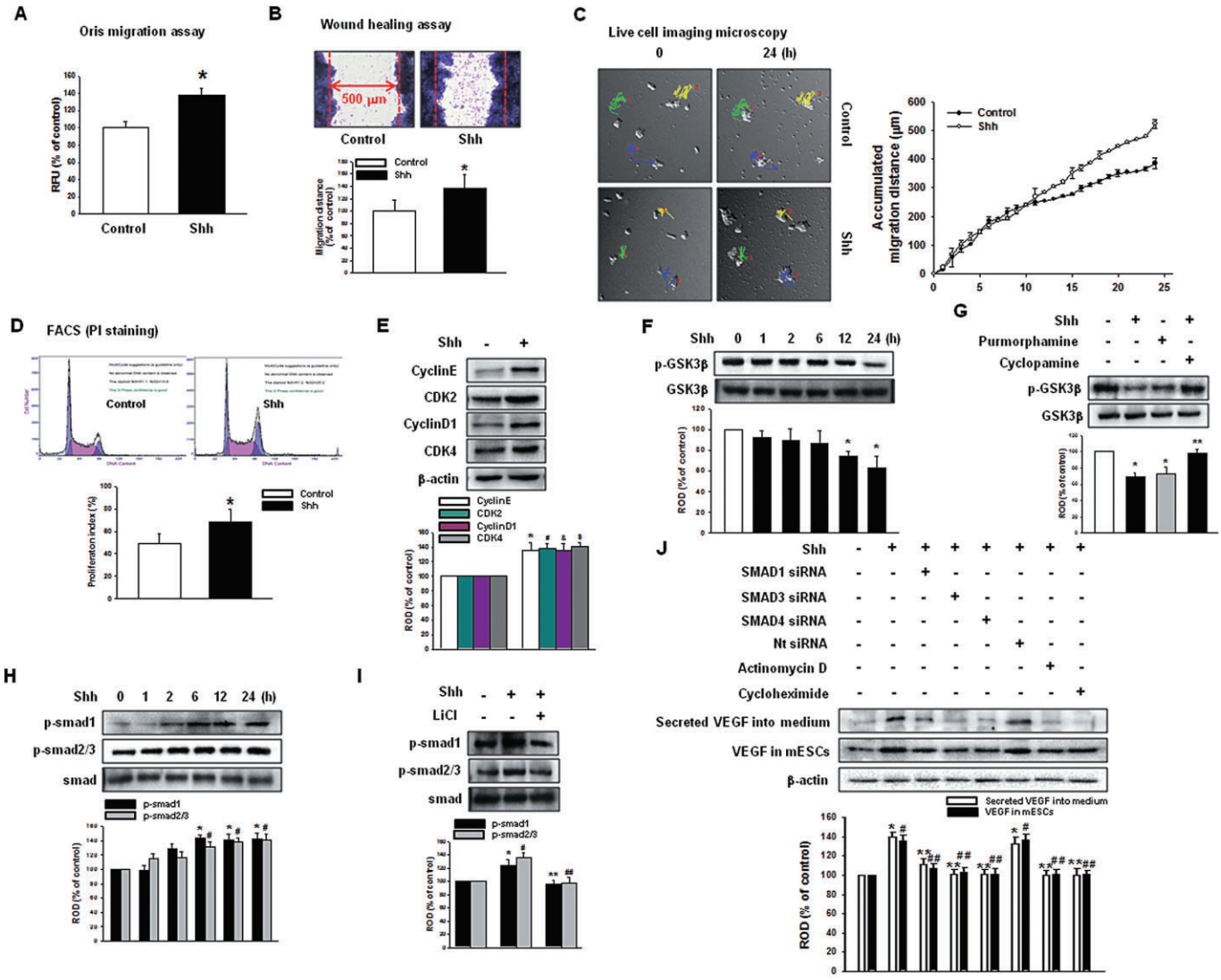

Figure 2

Effect of shh on mESC migration and proliferation *in vitro*. mESCs were treated with shh for 24 h. (A) Oris Cell Migration assay was performed and stained with calcein-AM (5 μM). Fluorescence in the analytical zone was quantified with a plate reader. (B) Wound-healing migration assay was performed and stained with Diff-Quik. Data represent the mean ± SD of three independent experiments with triplicate dishes. *$P < 0.05$ versus control. (C) Live cell imaging microscopy shows directed migration of mESCs under influence of shh. Coloured line and number in image indicate the tracked cells to measure the migration distance and the graph denotes the accumulated distance of migration analysed by the multidimensional acquisition package of Meta Morph v.7.01 software (Molecular Devices). (D) mESCs were subjected to PI staining for cell cycle analysis by flow cytometry. The gates were configured manually to determine the percentage of cells in S phase based on the DNA content. The data is calculated using proliferation index [(S + G2/M)/(G0/G1 + S + G2/M)] × 100 and reported as the mean ± SD of four independent experiment, each conducted in triplicate. *$P < 0.05$ versus control. (E) Protein expression of cyclin E, CDK2, cyclin D1 and CDK4 were detected by immunoblot. The lower panel depicts the mean ± SD of four independent experiments for each condition, as determined from densitometry relative to β-actin. *P, $^{\#}P$, $^{\&}P$, $^{\$}P < 0.05$ versus control. (F) mESCs were treated with shh for various time (0–24 h), and the expression of p-GSK3β was detected by immunoblot. (G) mESCs were treated with cyclopamine (SMO inhibitor; 10^{-5} M) prior to shh treatment for 24 h or cells were treated with purmorphamine (SMO agonist; 10^{-5} M) for 24 h and expression of p-GSK3β was detected by immunoblot. The lower panel depicts the mean ± SD of four independent experiments for each condition, as determined from densitometry relative to GSK3β. *$P < 0.05$ versus control; **$P < 0.05$ versus shh. (H) mESCs were treated with shh for various times (0–24 h), and the expression of p-Smad1 and p-Smad2/3 were detected by immunoblot. (I) mESCs were treated with LiCl (GSK3β inhibitor; 10^{-5} M) prior to shh treatment for 24 h, and the expression of p-Smad1 and p-Smad2/3 were detected by immunoblot. The lower panel depicts the mean ± SD of four independent experiments for each condition, as determined from densitometry relative to Smad. *$P < 0.05$ versus control of p-Smad1; **$P < 0.05$ versus shh of p-Smad1; $^{\#}P < 0.05$ versus control of p-Smad2/3; $^{\#\#}P < 0.05$ versus shh of p-Smad2/3. (J) mESCs were transfected with Smad1 siRNA (20 nM), Smad3 siRNA (20 nM), Smad4 siRNA (20 nM) or Nt siRNA (20 nM) for 24 h prior to shh treatment for 24 h and the VEGF secreted into the medium and the expression of VEGF in mESCs were detected by immunoblot. The lower panel depicts the mean ± SD of three independent experiments for each condition, as determined from densitometry relative to β-actin. *$P < 0.05$ versus control of secreted VEGF into medium; **$P < 0.05$ versus shh of secreted VEGF into medium; $^{\#}P < 0.05$ versus control of VEGF in mESCs; $^{\#\#}P < 0.05$ versus shh of VEGF in mESCs.

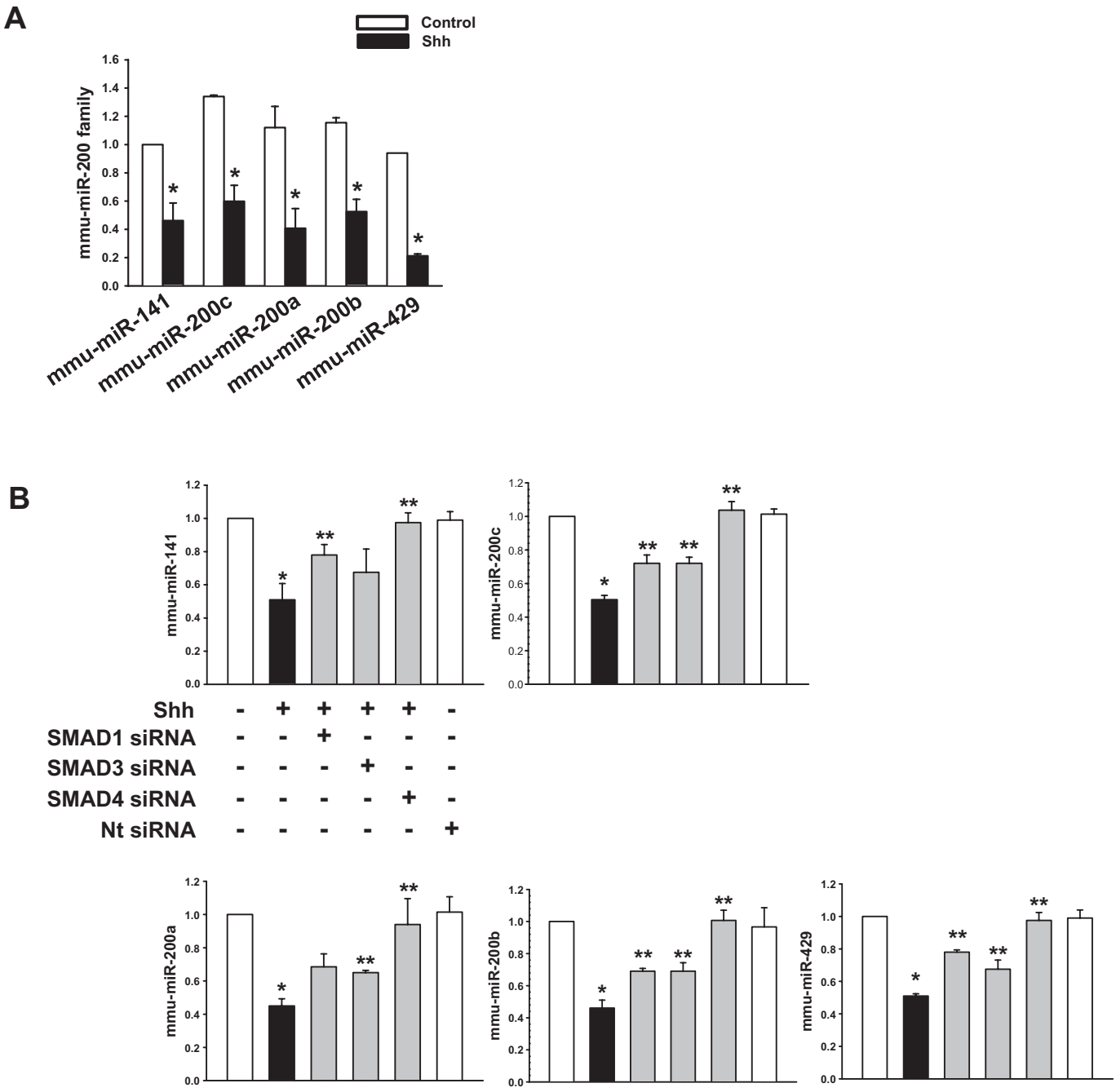

Figure 3

Effect of shh on miR-200 family. (A) mESCs were treated with shh for 24 h and the expression level of mmu-miR-141, -200c, -200a, -200b, -429 examined, using qRT-PCR. (B) mESCs were transfected with Smad1 siRNA, Smad3 siRNA, Smad4 siRNA or Nt siRNA for 24 h prior to shh treatment for 24 h and the expression level of mmu-miR-141, -200c, -200a, -200b, -429 examined using qRT-PCR. Data represents the mean ± SD of three independent experiments with triplicate dishes. *$P < 0.05$ versus control; **$P < 0.05$ versus shh.

the opposite of the ZEBs, which indicates a reciprocal inhibition between the two proteins (Figure 4A). To confirm the relationship between mmu-miR-141, -200b and ZEBs, we performed ChIP. First, protein–chromatin binding specificity was examined using agarose gel electrophoresis of input (non-immunoprecipitated chromatin; lane 1, 4), RNA polymerase antibody (positive control; lane 2), IgG antibody (same species as target antibody; negative control; lane 3) and specific antibody binding using ZEB1 antibody (target protein antibody; lane 5~6; Figure 4B). Next, ChIP-qPCR measured the levels of E-cadherin gene promoter binding with ZEB1. Figure 4C shows shh and mmu-miR-141, -200b hairpin inhibitor increased the ZEB1 binding with the E-cadherin gene promoter while the mmu-miR-141, -200b mimic

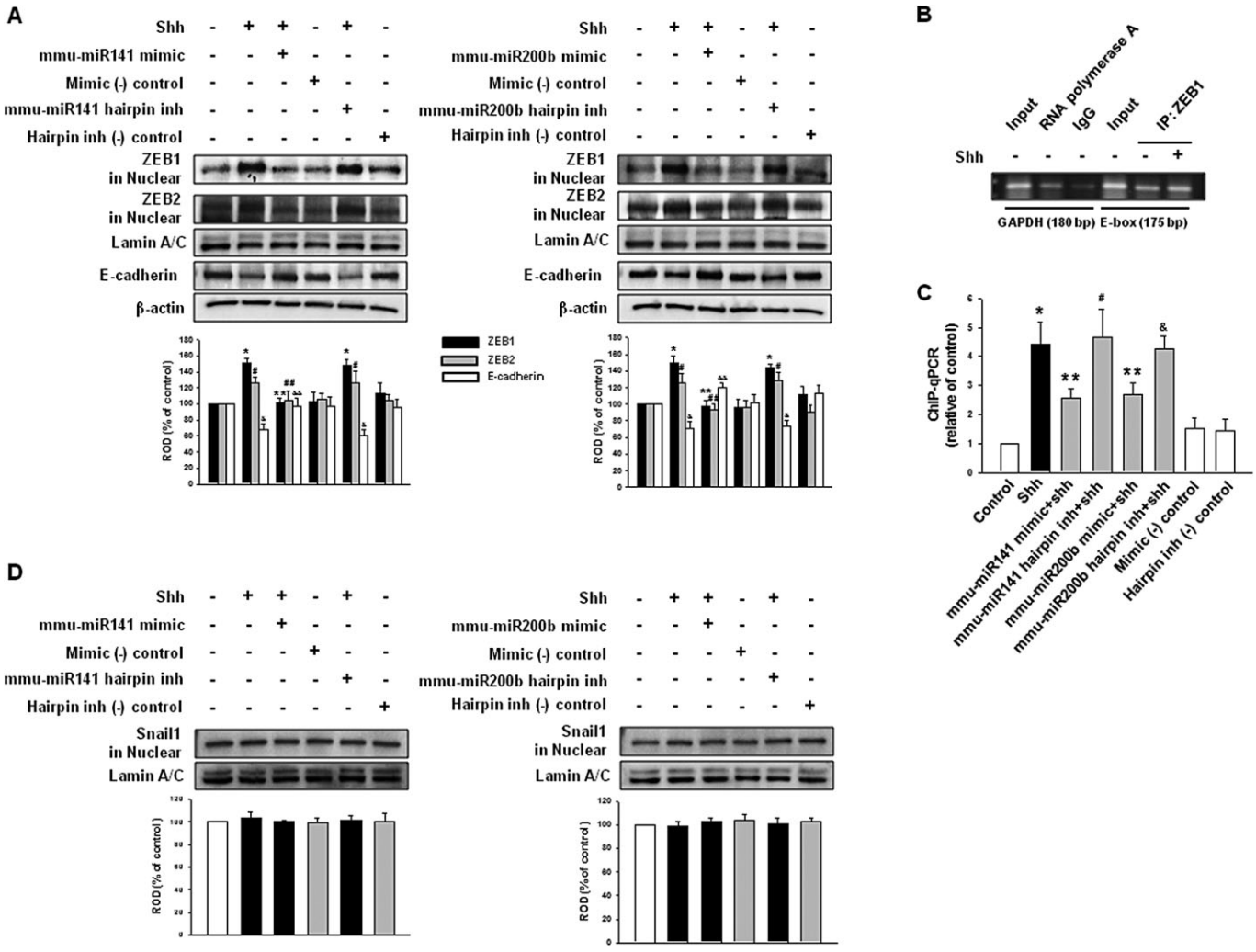

Figure 4

Feedback loop of miR-200 family–ZEB–E-cadherin. mESCs were transfected with mmu-miR-141 mimic (200 nM), mmu-miR-141 hairpin inhibitor (200 nM), mmu-miR-200b mimic (200 nM), mmu-miR-200b hairpin inhibitor (200 nM), mimic negative control [mimic (-) control; 200 nM] or hairpin inhibitor negative control [hairpin inh (-) control; 200 nM] for 24 h prior to shh treatment for 24 h. (A) The expression of ZEB1, ZEB2 in nuclear fraction or E-cadherin was detected by immunoblot. The lower panel depicts the mean ± SD of three independent experiments for each condition, as determined from densitometry relative to Lamin A/C or β-actin. $^{*}P < 0.05$ versus control of ZEB1; $^{**}P < 0.05$ versus shh of ZEB1; $^{\#}P < 0.05$ versus control of ZEB2; $^{\#\#}P < 0.05$ versus shh of ZEB2; $^{\&}P < 0.05$ versus control of E-cadherin; $^{\&\&}P < 0.05$ versus shh of E-cadherin. (B) Control ChIP assay. Input (non-immunoprecipitated chromatin lysate), anti-RNA polymerase (positive control) and IgG (negative control) or ZEB1 antibodies, which were immunoprecipitated with chromatin loaded in agarose gel. (C) ChIP assay. E-cadherin gene promoter binding with ZEB1 was assayed. The same input DNA was used for each ChIP assay and the values were normalized by input and the relative control was set at one. $^{*}P$, $^{\#}P$, $^{\&}P < 0.05$ versus control; $^{**}P < 0.05$ versus shh. (D) The expression of Snail1 in the nuclear fraction was detected by immunoblot. The lower panel shows the mean ± SD of three independent experiments for each condition, as determined from densitometry relative to Lamin A/C.

decreased binding. These results are consistent with the notion that ZEB1 represses E-cadherin by binding directly to their promoters. Zinc-finger transcription factors, from snails or slugs, repress E-cadherin transcription along with ZEBs (Hajra *et al.*, 2002). The specificity of the miR-200 family on ZEBs expression was confirmed by another E-cadherin gene promoter-binding protein: Snail1. Neither the shh nor mmu-miR-141, -200b hairpin inhibitor affected Snail1 expression (Figure 4D).

To check if the miR-200 family was involved in cell migration, we used the Oris migration assay and wound-healing assay. As shown in Figure 5A and B, shh and mmu-miR-141, -200b hairpin inhibitor increased cell movement. Shh decreased β-catenin/E-cadherin (adherent junction), ZO-1/occludin (tight junction) and ZO-1/Cx43 (gap junction) complexes during experimental observations. However, mmu-miR-141, -200b hairpin inhibitor and mmu-miR-141, -200b mimic did not influence ZO-1/occludin and ZO-1/Cx43 (Figure 5C). These results suggest that decreased E-cadherin modulated mESC migration. To examine the effect of miR-141/200b on skin wound, cells were transfected with microRNA mimics or mimic negative control. Mimic negative

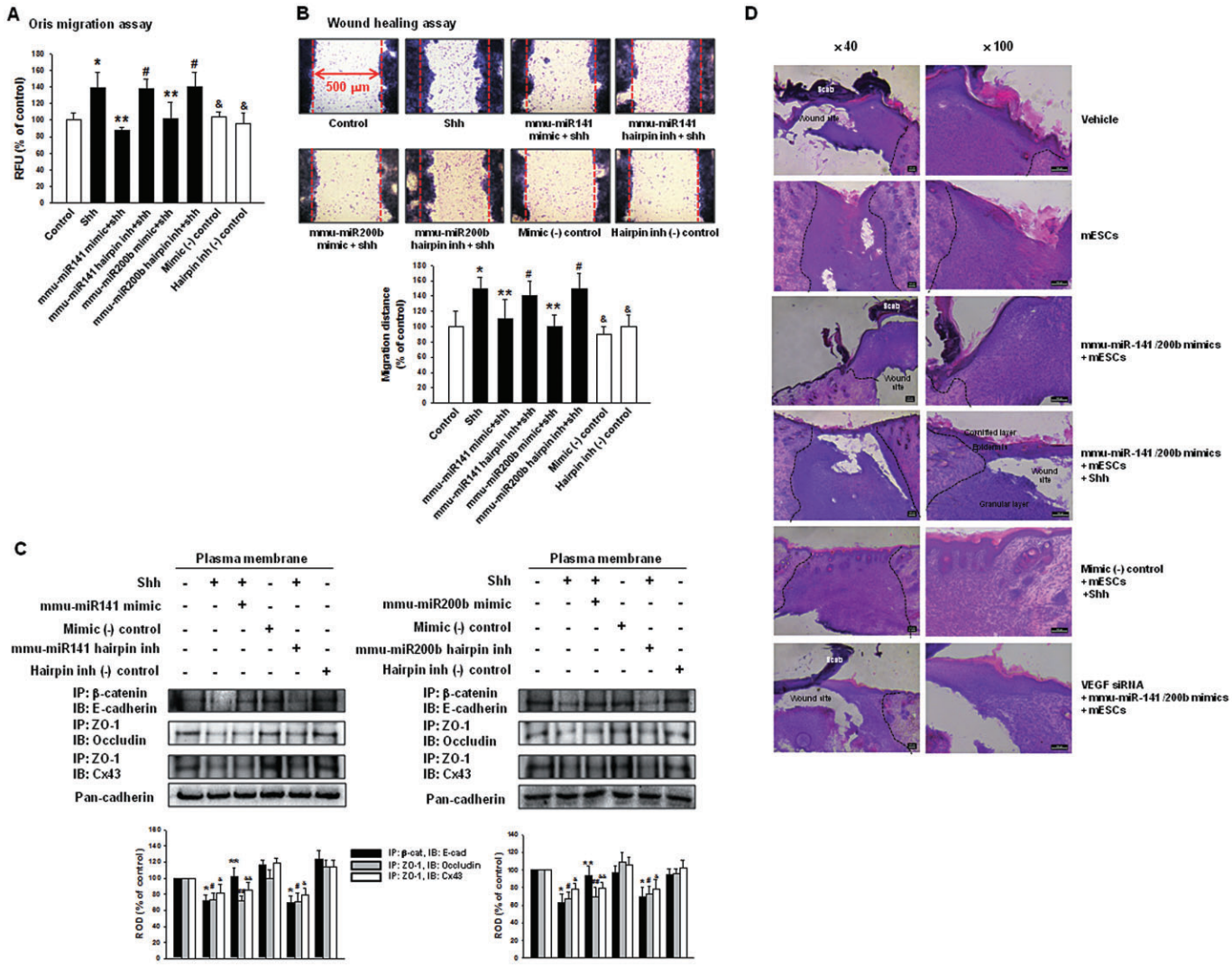

Figure 5

Involvement of miR-200 family in mESC migration and skin wound healing. mESCs were transfected with mmu-miR-141 mimic, mmu-miR-141 hairpin inhibitor, mmu-miR-200b mimic, mmu-miR-200b hairpin inhibitor, mimic negative control or hairpin inhibitor negative control for 24 h prior to shh treatment for 24 h. (A) Oris Cell Migration assay was performed and stained with calcein-AM (5 μM). Fluorescence in the analytical zone was quantified with a plate reader. (B) Wound-healing migration assay was performed and stained with Diff-Quik. Data represent the mean ± SD of three independent experiments with triplicate dishes. $^{*}P$, $^{\#}P$, $^{\&}P < 0.05$ versus control; $^{**}P < 0.05$ versus shh. (C) Immunoprecipitation and immunoblot. Plasma membrane protein lysates were immunoprecipitated with an anti-E-cadherin, anti-ZO-1 antibody and blotted with antibodies directed against β-catenin, occludin or Cx43 respectively. The example shown is representative of three independent experiments. The expression level of pan-cadherin in plasma membrane protein lysates were used as loading control. IgG was used for negative control (data not shown).$^{*}P < 0.05$ versus control of IP: β-cat, IB: E-cad; $^{**}P < 0.05$ versus shh of IP: β-cat, IB: E-cad; $^{\#}P < 0.05$ versus control of IP: ZO-1, IB: occludin; $^{\#\#}P < 0.05$ versus shh of IP: ZO-1, IB: occludin; $^{\&}P < 0.05$ versus control of IP: ZO-1, IB: Cx43; $^{\&\&}P < 0.05$ versus shh of IP: ZO-1, IB: Cx43. (D) Vehicle, mESCs, mmu-miR-141/200b mimics-transfected mESCs (mmu-miR-141/200b mimics + mESCs), mmu-miR-141/200b mimics-transfected mESCs with shh (mmu-miR-141/200b mimics + mESCs + shh), mimic negative control-transfected mESCs with shh [mimic (-) control + mESCs + shh] or both VEGF siRNA and mmu-miR-141/200b mimics-transfected mESCs (VEGF siRNA + mmu-miR-141/200b mimics + mESCs) were applied to skin wounds. Representative haematoxylin and eosin staining of wound skin at day 9 after wounding. Scale bar = 100 μm.

control-transfected mESCs with shh group [mimic (-) control + mESCs + shh] showed complete skin wound healing while mmu-miR-141/200b mimics-transfected mESCs group (mmu-miR-141/200b mimics + mESCs) and miR-141/200b mimics-transfected mESCs with shh group (mmu-miR-141/200b mimics + mESCs + shh) showed partial skin wound healing. Both VEGF siRNA and mmu-miR-141/200b mimics-transfected mESCs groups (VEGF siRNA + mmu-miR-141/200b mimics + mESCs) had less compact granular layers than mmu-miR-141/200b mimics-transfected mESCs groups (Figure 5D). This result suggests that both mESC migration and VEGF synthesis were important for skin wound healing. We confirmed the direct reciprocal inhibition between ZEB1 and E-cadherin. Immunoblotting and immunofluorescence staining showed that the endogenous depletion of ZEB1 reversed shh-induced decrease of E-cadherin expression

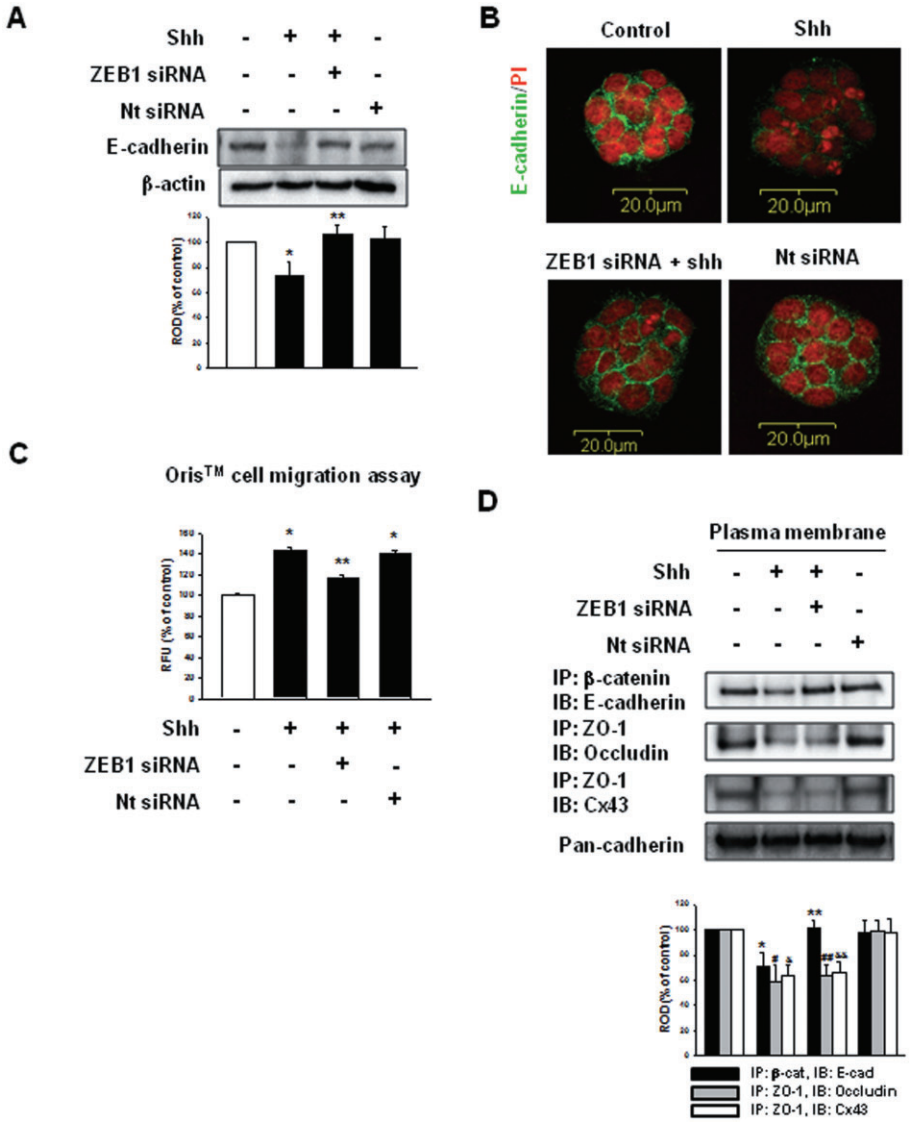

Figure 6

Involvement of ZEB1 in mESC migration and cell–cell junctions. mESCs were transfected with ZEB1 siRNA (20 nM) or Nt siRNA (20 nM) for 24 h prior to shh treatment for 24 h. (A and B) The expression of E-cadherin was detected by immunoblot and immunofluorescence staining. The lower panel depicts the mean ± SD of three independent experiments for each condition, as determined from densitometry relative to β-actin. $^{*}P < 0.05$ versus control; $^{**}P < 0.05$ versus shh. (C) Oris Cell Migration assay was performed and stained with calcein-AM (5 μM). Fluorescence in the analytical zone was quantified with a plate reader. Data represent the mean ± SD of three independent experiments with triplicate dishes. $^{*}P < 0.05$ versus control; $^{**}P < 0.05$ versus shh. (D) Immunoprecipitation and immunoblot. Plasma membrane protein lysates were immunoprecipitated with an anti-E-cadherin, anti-ZO-1 antibodies and blotted with antibodies directed against β-catenin, occludin or Cx43 respectively. The example shown is representative of three independent experiments. The expression level of pan-cadherin in plasma membrane protein lysates was used as loading control. $^{*}P < 0.05$ versus control of IP: β-cat, IB: E-cad; $^{**}P < 0.05$ versus shh of IP: β-cat, IB: E-cad; $^{\#}P < 0.05$ versus control of IP: ZO-1, IB: occludin; $^{\#\#}P < 0.05$ versus shh of IP: ZO-1, IB: occludin; $^{\&}P < 0.05$ versus control of IP: ZO-1, IB: Cx43; $^{\&\&}P < 0.05$ versus shh of IP: ZO-1, IB: Cx43.

(Figure 6A and B). ZEB1 siRNA inhibited cell migration (Figure 6C) also increased the β-catenin/E-cadherin complex (Figure 6D).

Discussion and conclusions

Earlier studies have reported the advantages of using exogenous stem cells to heal wounds. For example, Nakagawa *et al*. (2005) showed that MSCs with basic fibroblast growth factor promoted wound healing in a skin defect model, and Lee *et al*. (2011) reported that topical ESC application accelerates wound healing in the early stages of diabetes. These reports suggest that stem cells are an effective treatment for skin injuries and soluble factors may support the role of stem cells. In our *in vivo* study, we found that mESCs with shh accelerated skin wound healing, compared with the effects of mESCs alone. Shh indirectly up-regulates the angiogenic

factor, VEGF, which allows new blood vessel development to promote blood flow to wounded skin (Pola *et al.*, 2001; Fujita *et al.*, 2009; Teng *et al.*, 2012). Our results showed that VEGF siRNA impaired the wound-healing effect of mESCs by shh. This suggests that shh inhibition delays wound closure or disruption. As self-renewal of mESCs is important to the wound-healing process, we examined the underlying mechanisms of shh-induced mESCs migration and proliferation.

Shh regulates self-renewal in mESCs through canonical or non-canonical hedgehog pathways, which are related to SMO (Heo *et al.*, 2007). As SMO is associated with the serine/threonine kinases in the C-terminal (Aikin *et al.*, 2008), various hedgehog signalling components like GSK3β and Smads are phosphorylated on several residues. Smads are generally known as positive regulators of stem cell self-renewal (Karlsson *et al.*, 2007; Lee *et al.*, 2012), but they also regulate miRNA biosynthesis. ChIP analysis reveals that miRNA promoter elements and protein coding regions closely resemble each other (Ozsolak *et al.*, 2008), so Smads are expected to control gene transcription of various miRNAs. Shh-induced decrease of mmu-miR-141, -200c, -200a, -200b, -429 expressions were completely reversed by Smad4 siRNA, while Smad1 or Smad3 inhibition only slightly reversed miRNA expression decrease. Ahn *et al.* (2012) reported that Smad3 transactivates miR 200 expression in gastric cancer cells while decreasing miR 200a, 200c, 429, 200a and 141 expression levels depending on the type of activated Smad signalling (Xiong *et al.*, 2012). Although there is a discrepancy between the Smad and miR 200 family, our results suggest that shh mediates the negative transcriptional regulation of miRNA expression through the R-Smad (Smad1, Smad2/3)/Co-Smad (Smad4) heterodimer in nuclear localization. Boström *et al.* (2004) reported that activated Smad up-regulates VEGF expressionand others found that the phosphorylation of Smad2 and Smad3 was related to VEGF synthesis through Smad 2, -3 and -4 binding with the VEGF promoter (Clifford *et al.*, 2008). Our results showed that shh-induced increase of Smad1 and Smad2/3 phosphorylation was related to VEGF synthesis which is consistent with our previous study.

The role of the miR-200 family in ESC pluripotency has not been clear until now. It directly targets cadherin and regulated the mRNA expression of the transcriptional repressor ZEB1 in cancer cells (Bracken *et al.*, 2008; Saydam *et al.*, 2009). The miR-200 family is assumed to be important in stalling mESCs migration. Reducing mmu-miR-141, -200b leads to increased levels of ZEB1 in nucleus and blocks E-cadherin expression. Furthermore, the miR-200 family and ZEBs organized complementary signalling pathways to regulate E-cadherin. A decrease in E-cadherin changes the cellular structure and plasma membrane-associated protein localization as well as increasing cell motility in ESCs (Spencer *et al.*, 2007). Mmu-miR-141, -200b affected the E-cadherin/β-catenin (adherent junction) complex while ZO-1/occludin (tight junction) or ZO-1/Cx43 (gap junction) did not change, which points towards the miR-200 family as being responsible for fine tuning E-cadherin expression only in mESCs. Although we did not examine the relationship between migration and tight junctions or gap junctions, our results strongly suggest that the shh-induced decrease of cell–cell junctions were related to migration. In experiments that examined the relation between cell migration and wound healing, mmu-miR-141/200b mimics-transfected mESCs group showed partial skin wound healing. In conclusion, mESCs exhibited an accelerated skin wound healing in the presence of shh, through the mmu-miR-141, -200b-dependent down-regulation of E-cadherin. Shh can possibly lead to future developments in stem cell therapy.

Acknowledgements

This research was supported by the National Research Foundation of Korea (NRF) funded by the Ministry of Education (2013M3A9B4076520, 2013R1A6A301065444) and the Next-Generation BioGreen 21 Program (No. PJ009090), Rural Development Administration, Republic of Korea.

Author contributions

H.N.S. contributed to the conception and design, conduct the experiment, collection and assembly of data, data analysis and interpretation, as well as manuscript writing. H.J.H. contributed to the conception and design, administrative support, manuscript writing and final approval of manuscript.

Conflict of interest

None.

References

Ahn S, Joyner AL (2005). *In vivo* analysis of quiescent adult neural stem cells responding to sonic hedgehog. Nature 437: 894–897.

Ahn SM, Cha JY, Kim J, Kim D, Trang HT, Kim YM *et al.* (2012). Smad3 regulates E-cadherin via miRNA-200 pathway. Oncogene 31: 3051–3059.

Aikin RA, Ayers KL, Thérond PP (2008). The role of kinases in the hedgehog signalling pathway. EMBO Rep 9: 330–336.

Alexander SPH, Benson HE, Faccenda E, Pawson AJ, Sharman JL, Spedding M *et al.* (2013a). The Concise Guide to PHARMACOLOGY 2013/14: Enzymes. Br J Pharmacol 170: 1797–1867.

Alexander SPH, Benson HE, Faccenda E, Pawson AJ, Sharman JL, Spedding M *et al.* (2013b). The Concise Guide to PHARMACOLOGY 2013/14: G Protein-Coupled Receptors. Br J Pharmacol 170: 1459–1581.

Asano T, Ageyama N, Takeuchi K, Momoeda M, Kitano Y, Sasaki K *et al.* (2003). Engraftment and tumor formation after allogeneic *in utero* transplantation of primate embryonic stem cells. Transplantation 76: 1061–1067.

Bhardwaj G, Murdoch B, Wu D, Baker DP, Williams KP, Chadwick K *et al.* (2001). Sonic hedgehog induces the proliferation of primitive human hematopoietic cells via BMP regulation. Nat Immunol 2: 172–180.

Bitgood MJ, Shen L, McMahon AP (1996). Sertoli cell signaling by Desert hedgehog regulates the male germline. Curr Biol 6: 298–304.

Blahna MT, Hata A (2012). Smad-mediated regulation of microRNA biosynthesis. FEBS Lett 586: 1906–1912.

Boström K, Zebboudj AF, Yao Y, Lin TS, Torres A (2004). Matrix GLA protein stimulates VEGF expression through increased transforming growth factor-β1 activity in endothelial cells. J Biol Chem 279: 52904–52913.

Bracken CP, Gregory PA, Kolesnikoff N, Bert AG, Wang J, Shannon MF *et al.* (2008). A double-negative feedback loop between ZEB1-SIP1 and the microRNA-200 family regulates epithelial-mesenchymal transition. Cancer Res 68: 7846–7854.

Burk U, Schubert J, Wellner U, Schmalhofer O, Vincan E, Spaderna S *et al.* (2008). A reciprocal repression between ZEB1 and members of the miR-200 family promotes EMT and invasion in cancer cells. EMBO Rep 9: 582–589.

Calabrese JM, Seila AC, Yeo GW, Sharp PA (2007). RNA sequence analysis defines Dicer's role in mouse embryonic stem cells. Proc Natl Acad Sci U S A 104: 18097–18102.

Carpenter D, Stone DM, Brush J, Ryan A, Armanini M, Frantz G *et al.* (1998). Characterization of two patched receptors for the vertebrate hedgehog protein family. Proc Natl Acad Sci U S A 95: 13630–13634.

Chen L, Tredget EE, Wu PY, Wu Y (2008). Paracrine factors of mesenchymal stem cells recruit macrophages and endothelial lineage cells and enhance wound healing. PLoS ONE 3: e1886.

Chiang C, Litingtung Y, Lee E, Young KE, Corden JL, Westphal H *et al.* (1996). Cyclopia and defective axial patterning in mice lacking Sonic hedgehog gene function. Nature 383: 407–413.

Clifford RL, Deacon K, Knox AJ (2008). Novel regulation of vascular endothelial growth factor-A (VEGF-A) by transforming growth factor β1: requirement for Smads, β-CATENIN, AND GSK3β. J Biol Chem 283: 35337–35353.

Coraux C, Hilmi C, Rouleau M, Spadafora A, Hinnrasky J, Ortonne JP *et al.* (2003). Reconstituted skin from murine embryonic stem cells. Curr Biol 13: 849–853.

D'Amour KA, Agulnick AD, Eliazer S, Kelly OG, Kroon E, Baetge EE (2005). Efficient differentiation of human embryonic stem cells to definitive endoderm. Nat Biotechnol 23: 1534–1541.

Delloye-Bourgeois C, Gibert B, Rama N, Delcros JG, Gadot N, Scoazec JY *et al.* (2013). Sonic Hedgehog promotes tumor cell survival by inhibiting CDON pro-apoptotic activity. PLoS Biol 11: e1001623.

Eastham AM, Spencer H, Soncin F, Ritson S, Merry CL, Stern PL *et al.* (2007). Epithelial-mesenchymal transition events during human embryonic stem cell differentiation. Cancer Res 67: 11254–11262.

Fujita K, Miyamoto T, Saika S (2009). Sonic hedgehog: its expression in a healing cornea and its role in neovascularization. Mol Vis 15: 1036–1044.

Guo S, Dipietro LA (2010). Factors affecting wound healing. J Dent Res 89: 219–229.

Hajra KM, Chen DY, Fearon ER (2002). The SLUG zinc-finger protein represses E-cadherin in breast cancer. Cancer Res 62: 1613–1618.

Heo JS, Lee MY, Han HJ (2007). Sonic hedgehog stimulates mouse embryonic stem cell proliferation by cooperation of Ca^{2+}/protein kinase C and epidermal growth factor receptor as well as Gli1 activation. Stem Cells 25: 3069–3080.

Hochman E, Castiel A, Jacob-Hirsch J, Amariglio N, Izraeli S (2006). Molecular pathways regulating pro-migratory effects of Hedgehog signaling. J Biol Chem 281: 33860–33870.

Johnson RL, Scott MP (1998). New players and puzzles in the Hedgehog signaling pathway. Curr Opin Genet Dev 8: 450–456.

Karlsson G, Blank U, Moody JL, Ehinger M, Singbrant S, Deng CX *et al.* (2007). Smad4 is critical for self-renewal of hematopoietic stem cells. J Exp Med 204: 467–474.

Kilkenny C, Browne W, Cuthill IC, Emerson M, Altman DG (2010). Animal research: Reporting *in vivo* experiments: the ARRIVE guidelines. Br J Pharmacol 160: 1577–1579.

Korpal M, Lee ES, Hu G, Kang Y (2008). The miR-200 family inhibits epithelial-mesenchymal transition and cancer cell migration by direct targeting of E-cadherin transcriptional repressors ZEB1 and ZEB2. J Biol Chem 283: 14910–14914.

Lamouille S, Subramanyam D, Blelloch R, Derynck R (2013). Regulation of epithelial-mesenchymal and mesenchymal-epithelial transitions by microRNAs. Curr Opin Cell Biol 25: 200–207.

Lee KB, Choi J, Cho SB, Chung JY, Moon ES, Kim NS *et al.* (2011). Topical embryonic stem cells enhance wound healing in diabetic rats. J Orthop Res 29: 1554–1562.

Lee ST, Yun JI, van der Vlies AJ, Kontos S, Jang M, Gong SP *et al.* (2012). Long-term maintenance of mouse embryonic stem cell pluripotency by manipulating integrin signaling within 3D scaffolds without active Stat3. Biomaterials 33: 8934–8942.

Lin CH, Jackson AL, Guo J, Linsley PS, Eisenman RN (2009). Myc-regulated microRNAs attenuate embryonic stem cell differentiation. EMBO J 28: 3157–3170.

Liu P, Deng Z, Han S, Liu T, Wen N, Lu W *et al.* (2008). Tissue-engineered skin containing mesenchymal stem cells improves burn wounds. Artif Organs 32: 925–931.

Liu S, Dontu G, Mantle ID, Patel S, Ahn NS, Jackson KW *et al.* (2006). Hedgehog signaling and Bmi-1 regulate self-renewal of normal and malignant human mammary stem cells. Cancer Res 66: 6063–6071.

Marthiens V, Kazanis I, Moss L, Long K, Ffrench-Constant C (2010). Adhesion molecules in the stem cell niche – more than just staying in shape? J Cell Sci 123: 1613–1622.

McGrath J, Drummond G, McLachlan E, Kilkenny C, Wainwright C (2010). Guidelines for reporting experiments involving animals: the ARRIVE guidelines. Br J Pharmacol 160: 1573–1576.

Mitjavila-Garcia MT, Simonin C, Peschanski M (2005). Embryonic stem cells: meeting the needs for cell therapy. Adv Drug Deliv Rev 57: 1935–1943.

Nakagawa H, Akita S, Fukui M, Fujii T, Akino K (2005). Human mesenchymal stem cells successfully improve skin-substitute wound healing. Br J Dermatol 153: 29–36.

Ozsolak F, Poling LL, Wang Z, Liu H, Liu XS, Roeder RG *et al.* (2008). Chromatin structure analyses identify miRNA promoters. Genes Dev 22: 3172–3183.

Park SM, Gaur AB, Lengyel E, Peter ME (2008). The miR-200 family determines the epithelial phenotype of cancer cells by targeting the E-cadherin repressors ZEB1 and ZEB2. Genes Dev 22: 894–907.

Pawson AJ, Sharman JL, Benson HE, Faccenda E, Alexander SP, Buneman OP *et al.*; NC-IUPHAR (2014). The IUPHAR/BPS Guide to

PHARMACOLOGY: an expert-driven knowledge base of drug targets and their ligands. Nucl Acids Res 42 (Database Issue): D1098–D1106.

Pola R, Ling LE, Silver M, Corbley MJ, Kearney M, Blake Pepinsky R *et al.* (2001). The morphogen Sonic hedgehog is an indirect angiogenic agent upregulating two families of angiogenic growth factors. Nat Med 7: 706–711.

Ratajczak MZ, Kucia M, Jadczyk T, Greco NJ, Wojakowski W, Tendera M *et al.* (2012). Pivotal role of paracrine effects in stem cell therapies in regenerative medicine: can we translate stem cell-secreted paracrine factors and microvesicles into better therapeutic strategies? Leukemia 26: 1166–1173.

Rowitch DH, S-Jacques B, Lee SM, Flax JD, Snyder EY, McMahon AP (1999). Sonic hedgehog regulates proliferation and inhibits differentiation of CNS precursor cells. J Neurosci 19: 8954–8965.

Saydam O, Shen Y, Würdinger T, Senol O, Boke E, James MF *et al.* (2009). Downregulated microRNA-200a in meningiomas promotes tumor growth by reducing E-cadherin and activating the Wnt/β-catenin signaling pathway. Mol Cell Biol 29: 5923–5940.

Spencer HL, Eastham AM, Merry CL, Southgate TD, Perez-Campo F, Soncin F *et al.* (2007). E-cadherin inhibits cell surface localization of the pro-migratory 5T4 oncofetal antigen in mouse embryonic stem cells. Mol Biol Cell 18: 2838–2851.

Suh MR, Lee Y, Kim JY, Kim SK, Moon SH, Lee JY *et al.* (2004). Human embryonic stem cells express a unique set of microRNAs. Dev Biol 270: 488–498.

Teng H, Chopp M, Hozeska-Solgot A, Shen L, Lu M, Tang C *et al.* (2012). Tissue plasminogen activator and plasminogen activator inhibitor 1 contribute to sonic hedgehog-induced *in vitro* cerebral angiogenesis. PLoS ONE 7: e33444.

Tepass U, Harris KP (2007). Adherens junctions in Drosophila retinal morphogenesis. Trends Cell Biol 17: 26–35.

Wang X, Ge J, Tredget EE, Wu Y (2013). The mouse excisional wound splinting model, including applications for stem cell transplantation. Nat Protoc 8: 302–309.

Wu Y, Chen L, Scott PG, Tredget EE (2007). Mesenchymal stem cells enhance wound healing through differentiation and angiogenesis. Stem Cells 25: 2648–2659.

Xiong M, Jiang L, Zhou Y, Qiu W, Fang L, Tan R *et al.* (2012). The miR-200 family regulates TGF-β1-induced renal tubular epithelial to mesenchymal transition through Smad pathway by targeting ZEB1 and ZEB2 expression. Am J Physiol Renal Physiol 302: F369–F379.

Ying QL, Wray J, Nichols J, Batlle-Morera L, Doble B, Woodgett J *et al.* (2008). The ground state of embryonic stem cell self-renewal. Nature 453: 519–523.

Yoo YA, Kang MH, Kim JS, Oh SC (2008). Sonic hedgehog signaling promotes motility and invasiveness of gastric cancer cells through TGF-β-mediated activation of the ALK5-Smad 3 pathway. Carcinogenesis 29: 480–490.

Supporting information

Additional Supporting Information may be found in the online version of this article at the publisher's web-site:

http://dx.doi.org/10.1111/bph.12947

Figure S1 Examination of immune rejection markers in skin wound. Skin wounds at day 9 after wounding was acquired, and the expression of INF-γ or TNF-α was detected by immunoblot. The lower panel depicts the mean ± SD of three independent experiments for each condition, as determined from densitometry relative to β-actin.

Figure S2 Examination of transfection efficiency of siRNAs. mESCs were transfected with SMAD1 siRNA, SMAD3 siRNA, SMAD4 siRNA, ZEB1 siRNA or Nt siRNA and the expression of p-Smad1, p-Smad3, Smad4 or ZEB1 were detected by immunoblot.

Figure S3 Examination of the effect of mimic negative control and hairpin inhibitor negative control. mESCs were transfected with mimic negative control [mimic (-) control] or hairpin inhibitor negative control [hairpin inh (-) control] for 24 h prior to shh treatment for 24 h. Oris™ Cell Migration assay was performed and stained with calcein-AM (5 μM). Fluorescence in the analytical zone was quantified with a plate reader. Data represent the mean ± SD of three independent experiments with triplicate dishes. *$P < 0.05$ versus control.